Journal Name

COMMUNICATION

Highly Efficient Perovskite Solar Cells with Crosslinked PCBM Interlayers

Received 00th January 20xx,
Accepted 00th January 20xx

DOI: 10.1039/x0xx00000x

www.rsc.org/

W. Qiu, [a, b, †] J. P. Bastos, [a, c] S. Dasgupta, [a] T. Merckx, [a] I. Cardinaletti, [d] M. V. C. Jenart, [e] C. B. Nielsen, [e, f] R. Gehlhaar, [a] J. Poortmans, [a, c] P. Heremans, [a, c, †] I. McCulloch, [g] and D. Cheyns [a]

The commercially available phenyl-C_{61}-butyric acid methyl ester (PCBM) is crosslinked by 1,6-diazidohexane (DAZH), resulting in films resistant to common solvents used in perovskite solar cell processing. By using crosslinked PCBM as an interlayer and $(HC(NH_2)_2)_{0.66}(CH_3NH_3)_{0.34}PbI_{2.85}Br_{0.15}$ as the active layer, we achieve small area devices and modules with maximum steady-state power conversion efficiency of 18.1% and 14.9%, respectively.

By virtue of their rapid increasing power conversion efficiency (PCE) and potential for low-cost mass production, organometallic halide perovskite solar cells (PSCs) are promising candidate to challenge the photovoltaic market in the near future.[1] To date, the highest certified PCE of perovskite solar cells has reached 22.1%, which is close to the commercialized thin film counterparts such as CdTe based solar cells.[2]

Apart from the quality of the perovskite active layer, the stability and efficiency of PSCs depend also on the interlayers between electrodes and the active layer.[3,4] At the cathode side, high temperature (> 450 °C) annealed TiO_2 electron transport layers (ETLs) are commonly used in state-of-the-art PSCs.[5-7] However, such a high annealing temperature hinders the use of low-cost plastic substrates, and thus limits the potential for roll-to-roll production. Therefore, low temperature (<150 °C) processed n-type metal oxides like TiO_2,[8] ZnO,[4,9] SnO_2,[10] Zn_2SnO_4[11] have been widely explored in order to replace the high temperature annealed TiO_2.

In addition to n-type metal oxide interlayers, fullerenes such as phenyl-C_{61}-butyric acid methyl ester (PCBM) and C_{60} have proven to be excellent interlayers to improve the performance of PSCs.[4, 12-15] Such fullerene layers are usually incorporated in the so-called P-i-N structure perovskite solar cells, where the device fabrication starts with the deposition of hole transport layer on the substrates. The incorporation of fullerenes in N-i-P structures, where the device fabrication starts with the deposition of ETL on substrates, is limited by the lack of orthogonal solvent systems for device processing.[13] For example, PCBM can be dissolved and washed away from the substrate by *N*,*N*-dimethylformamide (DMF), a common solvent for perovskite precursors. To address this problem, fullerene derivatives with robust resistance against DMF have been synthesized, and applied to N-i-P structure perovskite solar cells to improve the electron extraction.[16-18] In this work, we introduce another approach to increase the solvent resistance of fullerenes by crosslinking commercial PCBM with 1,6-diazidohexane (DAZH).

[a] *IMEC, Kapeldreef 75, Heverlee, B-3001, Belgium*
[b] *MTM, KU Leuven, Heverlee, Belgium*
[c] *ESAT, KU Leuven, Heverlee, Belgium*
[d] *Hasselt University, IMO-IMOMEC, Diepenbeek, 3590, Belgium*
[e] *Department of Chemistry and Centre for Plastic Electronics, Imperial College London, SW7 2AZ, UK*
[f] *Materials Research Institute and School of Biological and Chemical Sciences, Queen Mary University of London, Mile End Road, London E1 4NS, UK*
[g] *Physical Sciences and Engineering Division, King Abdullah University of Science and Technology (KAUST), Thuwal 23955-6900 , Saudi Arabia*
† Corresponding author: Weiming.Qiu@imec.be; Paul.Heremans@imec.be
Electronic Supplementary Information (ESI) available. See DOI: 10.1039/x0xx00000x

DAZH can be synthesized in one step from readily available starting materials and has a good shelf-life.[19] Recently, McCulloch *et al* showed that a thin film of PCBM can be crosslinked by DAZH to form higher molecular weight fullerene

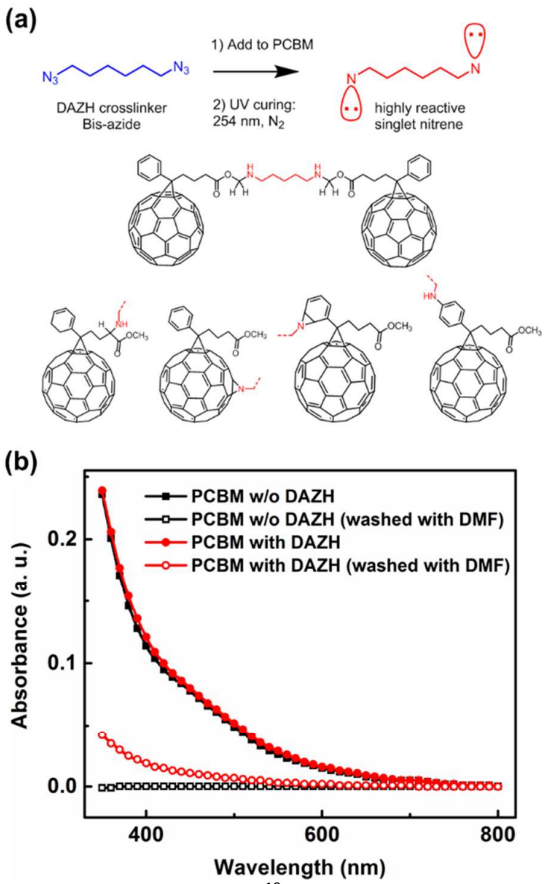

derivatives and oligomers.[19] Initiated by a UV light curing process, highly reactive nitrenes are formed from DAZH, which will react with neighboring PCBM molecules through C-H insertion. Though it is difficult to determine the exact insertion site, Fig. 1a illustrates an example of a crosslinking reaction as well as the potential reaction sites on PCBM molecules. The increased solvent resistance of the crosslinked PCBM layer relative to a neat PCBM layer can be demonstrated by UV-Vis spectroscopy. As is shown in Fig. 1b, the PCBM film without DAZH is completely removed after washing with DMF, with no detectable absorption from PCBM. In case of the crosslinked PCBM film with 15 wt% DAZH, there is still notable PCBM absorption observed, though the absorbance is 6 times lower. The thickness of the pristine PCBM film was measured to be 30 nm by Dektak. Assuming the absorption coefficient of PCBM is not affected by adding DAZH, we can calculate the thickness of the remaining crosslinked PCBM layer is about 5 nm according to the Lambert-Beer's law.

Fig. 1 (a) The photo-crosslinking mechanism and the possible reaction locations; (b) the UV-Vis spectra of the as-deposited PCBM films with and without DAZH, as well as the corresponding UV-Vis spectra after DMF washing. The DMF washing step was carried out after the UV curing process. The PCBM layers were deposited on ITO coated glass substrates.

To investigate the effect of the crosslinked PCBM interlayer on the performance of PSCs, devices with a structure of ITO/ETL/$CH_3NH_3PbI_3$/doped Spiro-OMeTAD/Au were fabricated. Fig. 2a compares the typical current density (*J*)-voltage (*V*) curves of devices without ETL, with pristine PCBM and with crosslinked PCBM from the reverse sweeps. The corresponding external quantum efficiency (EQE) curves of these three types of devices are shown in Fig. S1. The detailed photovoltaic parameters are listed in Table 1. The devices without ETL and with pristine PCBM give similar PCEs of 12.1% and 11.9% from *J-V* sweeps, respectively. This is consistent with the above UV-Vis results that indicate the removal of the pristine PCBM interlayer by DMF during the processing of the perovskite layer. However, for the device with crosslinked PCBM as ETL, the open circuit voltage (V_{oc}) and the fill factor (FF) are significantly improved, resulting in a superior PCE of 14.9%. Furthermore, the parasitic absorption from the thin 5 nm crosslinked PCBM film is low, and thus the short-circuit current density (J_{sc}) is not affected.

It is worth to note that hysteresis was observed for all these devices, though devices with crosslinked PCBM interlayer show less hysteresis under the same measurement condition (Fig. S2). In order to overcome the errors introduced by hysteresis and to have a more accurate assessment on device performance, the steady-state PCEs under constant voltage bias and continuous illumination were measured (Fig. 2b). The bias voltages were chosen to be the maximum power point voltages from the reverse *J-V* sweeps for each device. The devices without ETL and with pristine PCBM show much lower steady-state PCEs compared to the PCE values obtained from *J-V* sweeps. This is similar to the previous reported PSCs lacking selective charge transport layers.[20] The device with crosslinked PCBM, however, gives a steady-state PCE of 14.5% after 5 min operation, which is very close to the value measured from the reverse *J-V* sweep.

The aforementioned experiments indicate that the crosslinked PCBM interlayer survives the perovskite layer processing, and effectively improves the device performance. Nevertheless, with a HOMO level of -6.0 eV,[3] the hole blocking ability of PCBM is relatively poor. This can increase the chance of carrier recombination at the ITO/ETL interface and limits the further improvement of device performance. Therefore, in order to increase the carrier selectivity of the contact, an additional hole blocking layer was deposited between ITO and the crosslinked PCBM layer. Two types of hole blocking layers were chosen, i.e. TiO_2 and polyethyleneimine (PEIE), to assess the versatility of this approach. TiO_2 has a much deeper HOMO (-8.0 eV) compared to PCBM, while PEIE will create interfacial dipoles that block holes.[3]

Devices using TiO_2, TiO_2/crosslinked PCBM, PEIE, and PEIE/crosslinked PCBM as ETL were fabricated respectively,

while the active layer ($CH_3NH_3PbI_3$) and the hole transport layer (doped Spiro-OMeTAD) were kept the same. Fig. 2c shows the typical *J-V* curves of those devices from reverse sweeps, and the EQE curves are presented in Fig. S1b. The detailed photovoltaic parameters are also summarized in Table 1. Compared to the devices with only crosslinked PCBM as ETL, the V_{oc} of the devices with the double ETL is dramatically increased, which is consistent with our assumption that the additional hole blocking layer can reduce the interface recombination at the cathode. As a result, much higher PCEs of 17.1% and 16.5% can be achieved for these double ETL devices compared to the ones with crosslinked PCBM only. In addition, for both double ETL cases, the steady-state PCEs under constant bias are almost the same as the PCE values obtained from the reverse *J-V* sweeps (Fig. 2d). Moreover, perovskite solar cells with double ETL significantly outperform those with only TiO_2 or PEIE single ETL. The device with a single PEIE ETL barely works and shows a PCE of only 1.3%, while the device with a single TiO_2 ETL has a much lower steady-state PCE (12.9%) compared to the PCE measured from *J-V* sweep (15.8%). This again demonstrates the

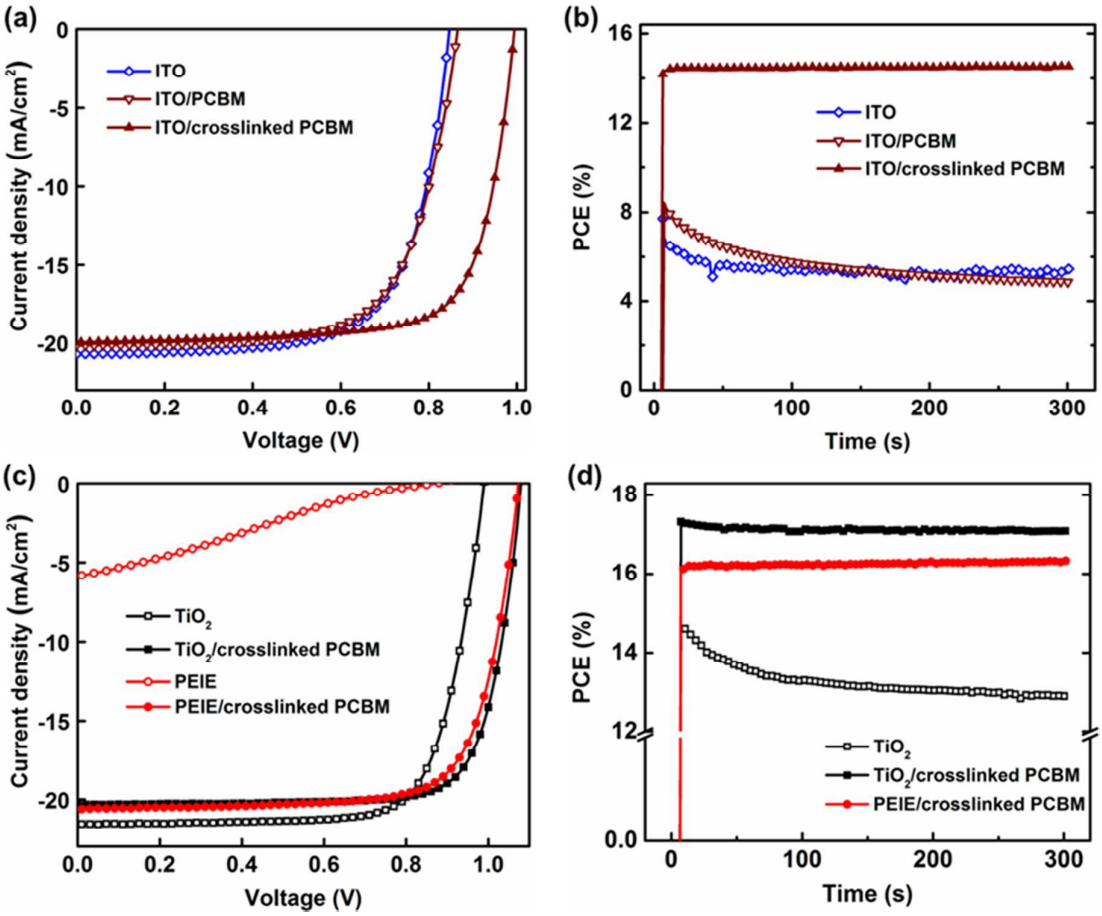

Fig. 2 (a) The *J-V* curves and (b) the steady-state PCEs of the PSCs without ETL, with pristine PCBM and with crosslinked PCBM as ETL; (c) The *J-V* curves and (d) the steady-state PCEs of PSCs with TiO_2, TiO_2/crosslinked PCBM, PEIE, PEIE/crosslinked PCBM as ETL.

Table 1. Summary of the detailed photovoltaic parameters of the perovskite solar cells using different ETLs. All these devices were made with structure of ITO/ETL/$CH_3NH_3PbI_3$/doped Spiro-OMeTAD/Au.

ETLs	J_{sc} (mA/cm^2)	$J_{sc,\ EQE}$ (mA/cm^2)	V_{oc} (V)	FF (%)	PCE_{jv} (%)	PCE_{bias} (%)	Irradiance (mW/cm^2)
ITO	20.7	18.8	0.85	68.5	12.1	5.5	100
PCBM	20.2	18.8	0.87	67.6	11.9	4.9	100
Crosslinked PCBM	20.0	19.2	0.99	74.6	14.9	14.5	99.3

TiO_2	21.6	18.7	0.99	74.5	15.8	12.9	100.4
TiO_2/crosslinked PCBM	20.3	19.5	1.08	77.9	17.1	17.1	100
PEIE	5.9	N/A	0.87	24.8	1.3	N/A	99.2
PEIE/crosslinked PCBM	20.6	19.6	1.07	74.9	16.5	16.3	100

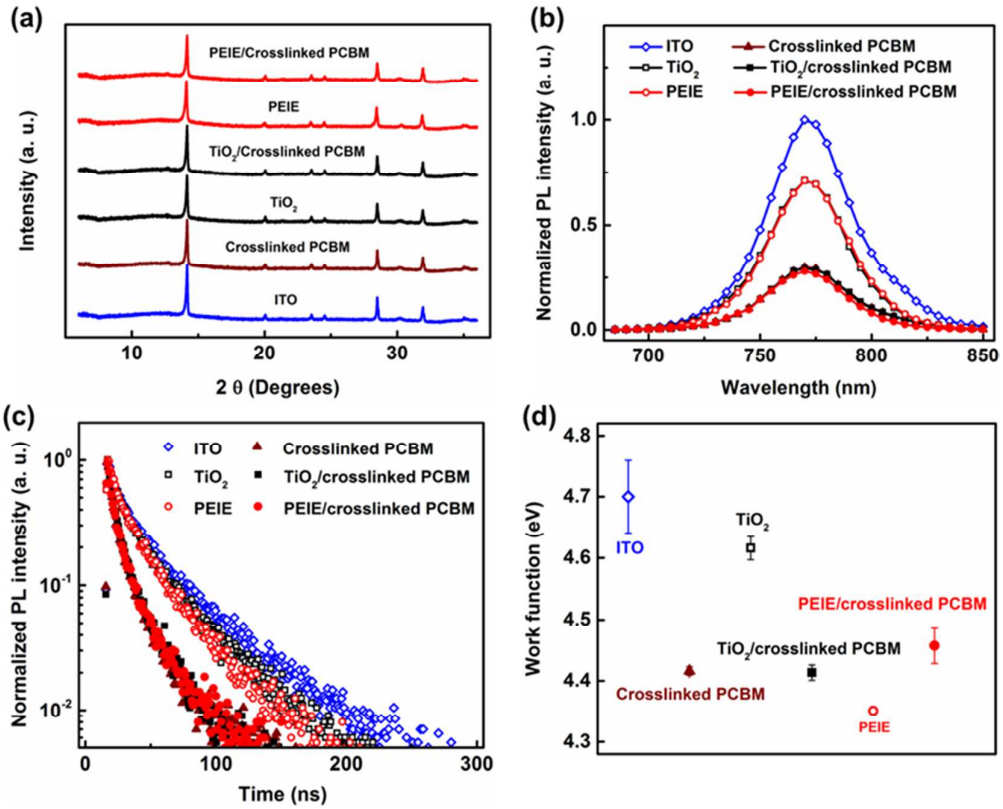

Fig. 3 (a) The XRD patterns of $CH_3NH_3PbI_3$ films deposited on different ETLs; (b) Steady-state PL spectra of the $CH_3NH_3PbI_3$ films on different ETLs; (b) time resolved PL measurements of the $CH_3NH_3PbI_3$ films on different ETLs, taken at the emission wavelength of 770 nm; (d) a comparison of the work function of different ETLs measured from KPFM, with the work function of ITO taken to be 4.7 eV.

effectiveness and versatility of the crosslinked PCBM interlayer in improving the performance of PSCs. Devices with pristine PCBM coated TiO_2 and PEIE ETLs were also fabricated. However, no significant improvement in performance was observed. The stead-state PCEs for devices with TiO_2/PCBM and PEIE/PCBM are 13.3% and 0.9%, respectively (Fig. S3 and Table S1).

It has been reported previously that the morphology of the perovskite layer shows a strong correlation with the underlying layer.[8,21,22] In order to gain more insight into how the crosslinked PCBM interlayer improves device performance, we investigated the morphologies of the $CH_3NH_3PbI_3$ layers made on different ETLs, by studying the X-ray diffraction (XRD) patterns and the top-view scanning electron microscope (SEM) images. From the XRD patterns (Fig. 3a), we find an identical perovskite crystal structure with similar peak intensities independent on the underlying ETL, indicating the crystallinity of the perovskite films is barely affected by the ETLs. From the top-view SEM images (Fig. S4), all the samples show a pinhole-free morphology. Small changes in grain size can be observed between the samples made on different ETLs, with the appearance of some large grains for the sample made on TiO2 without crosslinked PCBM. However, since the change of grain size is not significant, the effect of different grain sizes on device performance can be very limited. These observations

indicate that the enhanced performance of devices involving crosslinked PCBM may not be related to bulk morphological reasons, but it can be attributed to the better electron extraction from the perovskite layer to the crosslinked PCBM layer.

To give further evidence to this, steady-state photoluminescence (PL) quenching (Fig. 3b) and time-resolved PL decay measurements (Fig. 3c) were carried out for the $CH_3NH_3PbI_3$ films made on the different ETLs. This technique has been employed by different research groups to evaluate the carrier extraction from the active layer to the charge transport layer.[18,21,23-25] A higher PL quenching can be achieved when a crosslinked PCBM layer is under the $CH_3NH_3PbI_3$ layer, compared to the other cases. Correspondingly, the PL lifetime is also shorter when $CH_3NH_3PbI_3$ is interfaced with crosslinked PCBM, TiO_2/crosslinked PCBM, or PEIE/crosslinked PCBM. Considering the same quality of the $CH_3NH_3PbI_3$ bulk films, as indicated by XRD and SEM, the PL results are in line with our assumption that electron extraction from perovskite to the crosslinked PCBM layer is more efficient. In addition, although identical PL quenching and PL lifetime are measured for

Fig. 4 (a) J-V curves of the best device with the mixed perovskite measured with both reverse and forward sweeps, with the inset a cross-section SEM image of the mixed perovskite on ITO/TiO_2/crosslinked PCBM substrate; (b) The corresponding EQE curve; (c) the corresponding steady-state PCE under constant voltage bias and continuous illumination; (d) a PCE histogram of 96 devices.

$CH_3NH_3PbI_3$ on TiO_2 and PEIE, the device using only PEIE as ETL performs much worse than that using only TiO_2. This is probably because the PL quenching in the PEIE case is mainly related to surface recombination rather than charge transfer, which is indicated by the low V_{oc} and extremely low J_{sc}.

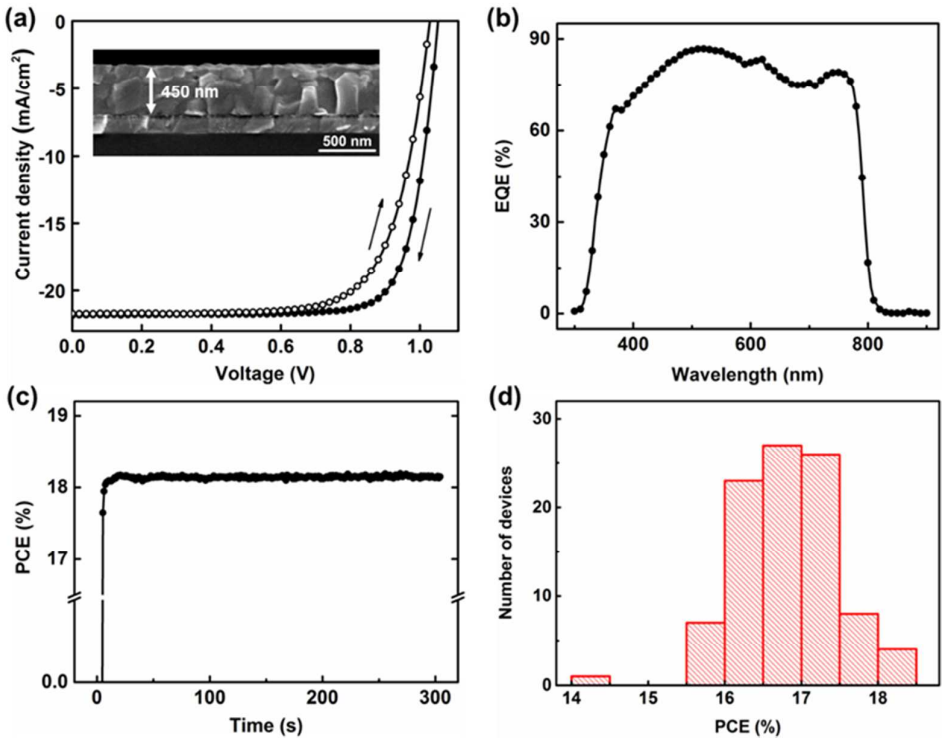

We further measured the work function of different ETLs on ITO substrates using Kelvin probe force microscopy (KPFM). The surface potential mapping images show that the surface potential is homogenous over the areas measured for each ETL (Fig. S5). Although the absolute work function values from KPFM measurement may not be accurate, the relative work function comparison between different layers is still valid. Here, we took the work function of ITO to be 4.7 eV as reported by literature,[3,26] and then correlated the average work functions of other ETLs from the KPFM measurements (averaged over the scanned areas) to the known value for ITO (Fig. 3d). As expected, all ETLs with crosslinked PCBM show similar work functions. A crosslinked PCBM layer on TiO_2 upshifts the work function of TiO_2 by about 0.2 eV. The lower work function of TiO_2/crosslinked PCBM may partially account for the improved V_{oc} of the corresponding devices. Interestingly, even though PEIE shows the lowest work function, the device based on PEIE performs poorly. On the contrary, the device based on PEIE/crosslinked PCBM shows much better performance, though the crosslinked PCBM downshifts the work function of PEIE by about 0.1 eV. As also indicated by the PL results, such an improved device

performance may be related to the reduced surface recombination at ETL/perovskite interface, due to the passivation effects of crosslinked PCBM.[18] Combining all the results from different characterizations, we believe the effects of crosslinked PCBM on the performance of perovskite solar cells are threefold: (1) increased electron extraction, (2) improved energy level alignment and (3) decreased surface recombination.

Recently, mixed perovskites such as $(HC(NH_2)_2)_{1-x}(CH_3NH_3)_xPbI_{3-y}Br_y$ are used to obtain more efficient photovoltaic cells compared to $CH_3NH_3PbI_3$.[5-7,27,28] Here, we screened the compatibility of these material systems with our new double ETL, using devices with a structure of ITO/TiO_2/crosslinked PCBM/$(HC(NH_2)_2)_{1-x}(CH_3NH_3)_xPbI_{3-y}Br_y$/doped Spiro-OMeTAD/ Au. Although it is difficult to determine the exact composition of our mixed perovskite layer, we calculated the composition from the ratio of the used precursors to be $(HC(NH_2)_2)_{0.66}(CH_3NH_3)_{0.34}PbI_{2.85}Br_{0.15}$, which is close to the optimal one reported by Hagfeldt *et al*.[27] Top-view (Fig. S6) and the cross-section (Fig. 4a, inset) SEM images show that smooth and pinhole-free films of this mixed perovskite material can be achieved, with a thickness of around 450 nm. Compared to $CH_3NH_3PbI_3$, the XRD peaks of $(HC(NH_2)_2)_{0.66}(CH_3NH_3)_{0.34}$ $PbI_{2.85}Br_{0.15}$ are slightly shifted to smaller diffraction angles, indicating the increase of lattice parameters due to the incorporation of $HC(NH_2)_2^+$ (Fig. S7).[28]

The *J-V* curves of our best device based on the above-mentioned mixed perovskite are presented in Fig. 4a. Measured with reverse sweep, it gives a PCE of 18.4% under 98.6 mW/cm^2 irradiance, with a J_{sc} of 21.9 mA/cm^2, a V_{oc} of 1.05 V, and a FF of 79.1%. Due to the hysteresis, an inferior PCE of 16.4% is obtained with forward sweep, with a J_{sc} of 21.7 mA/cm^2, a V_{oc} of 1.03 V, and a FF of 72.2%. The J_{sc} calculated from the EQE curve plotted in Fig. 4b is equal to 21.1 mA/cm^2, which is comparable to the value obtained from *J-V* sweep. Despite the device hysteresis, the steady-state PCE under constant bias and continuous illumination is close to the value measured with reverse *J-V* sweep, showing a PCE of 18.1% after 5 min operation (Fig. 4c). Moreover, a histogram of 96 devices from different substrates is given in Fig. 4d, indicating a narrow PCE distribution and good reproducibility of these devices. Such a homogeneity in device performance also enables us to fabricate large area perovskite solar modules with high aperture PCE, using the same layer stack. The perovskite solar module has the same design shown in our previous work, with an aperture area of 4 cm^2 (Fig. S8).[29] As is shown in Fig. S9a, our module gives a V_{oc} of 4.05 V, a short circuit current of 20 mA and a FF of 74%, resulting in a maximum power output of 59.9 mW with a 4 cm^2 aperture area. Since the irradiance is 100 mW/cm^2, the aperture PCE of our module equals to 14.9%. Moreover, an identical steady-state PCE of 14.9% is shown in Fig. S9b.

Conclusions

In summary, we have demonstrated that crosslinked PCBM layers are resistant against solvents like DMF, and can be used as efficient electron extraction interlayer to improve the performance of perovskite solar cells. Due to the relatively poor hole blocking ability, an additional hole blocking layer such as TiO_2 or PEIE is required under the crosslinked PCBM, in order to get the optimal device performance. With a mixed perovskite material, $(HC(NH_2)_2)_{0.66}(CH_3NH_3)_{0.34}PbI_{2.85}Br_{0.15}$, we are able to achieve small area perovskite solar cells with a maximum PCE of 18.4%, as well as 4 cm^2 perovskite solar modules with a maximum aperture PCE of 14.9%. Our approach of using crosslinked charge transport layers opens new direction to overcome the solvent incompatibility during device processing and also to design novel charge transport materials.

Experimental Section

Materials: The glass substrates with patterned ITO electrodes were obtained from Colorado Concept Coatings. PbI_2 powder was purchased from TCI Chemicals. CH_3NH_3I, CH_3NH_3Br, $CH(NH_2)_2I$ were obtained from Dyesol. PCBM and DAZH were received from Nano-C and Imperial College London, respectively. The synthesis of DAZH was reported in Reference 19. Spiro-OMeTAD was bought from Lumtec. Anhydrous solvents, i.e. DMF, dimethyl sulfoxide (DMSO), isopropanol, chlorobenzene were purchased from Sigma Aldrich.

Preparation of the ETLs: The pristine crosslinked PCBM layer was prepared by spin coating a 10 mg/mL PCBM solution in chlorobenzene onto ITO substrate at 2000 rpm. For the crosslinked PCBM layer, 10 mg/mL PCBM in chlorobenzene with the addition of 15 wt% DAZH was spin coated onto ITO substrate at 2000 rpm. Then, it was illuminated with UV light (254 nm) for 15 min for photo-crosslinking. The TiO_2 layer was evaporated at a rate of 1 Å/s onto ITO substrates by reactive electron beam evaporation. To maintain the stoichiometry of the film, a partial O_2 pressure of 1.7×10^{-4} Torr during the deposition was introduced. To get the PEIE layer, a 0.1 wt% PEIE solution in 2-methoxy ethanol was spin coated onto ITO at 3000 rpm, followed by a 10 min thermal annealing step at 100 °C.

Preparation of the perovskite layers: a two-step inter-diffusion method was applied to fabricate the perovskite layers. For $CH_3NH_3PbI_3$, a 461 mg/mL PbI_2 solution in DMF with a small portion of DMSO as additive (PbI_2:DMSO = 1:1, molar ratio), was first spin coated onto the substrate at 3000 rpm for 30 s. Then, a 50 mg/mL CH_3NH_3I solution in isopropanol was spin coated onto the PbI_2 layer at 3000 rpm for another 30 s. Afterwards, the substrate was annealed at 100 °C for 15 min in order to form the perovskite crystal structure. To make the $(HC(NH_2)_2)_{0.66}(CH_3NH_3)_{0.34}PbI_{2.85}Br_{0.15}$ films, the same procedure as for $CH_3NH_3PbI_3$ was followed, except the use of a mixed $CH(NH_2)_2I$, CH_3NH_3I and CH_3NH_3Br solution instead of pure CH_3NH_3I in isopropanol. The molar ratio of $CH(NH_2)_2I$, CH_3NH_3I and CH_3NH_3Br was kept 0.66: 0.19: 0.15.

Device fabrication: The ITO coated glass was cleaned with ultrasonic baths of detergent, deionized water, acetone, and isopropanol each for 10 minutes. Then, different ETLs were deposited according to the methods mentioned above. On the ETLs, $CH_3NH_3PbI_3$ or $(HC(NH_2)_2)_{0.66}(CH_3NH_3)_{0.34}PbI_{2.85}Br_{0.15}$ films was fabricated. The perovskite films were made in an N_2 filled glove box. After that, an 80 mg/mL Spiro-OMeTAD solution doped with 17.5 µl lithium bis(trifluoromethanesulfonyl) imide (520 mg/mL in acetonitrile) and 28.5 µL 4-tert-butylpyridine was spin-coated onto the perovskite films. The perovskite films coated with Spiro-OMeTAD were then exposed to air overnight for Spiro-OMeTAD oxygen doping. The small area devices were completed by depositing an 80 nm Au layer onto the Spiro-OMeTAD through shadow masks, defining an active area of 0.13 cm^2. The perovskite solar modules were fabricated using the same method described in our previous work.[29]

Characterizations: the UV-vis measurement was carried out on SHIMADZU UV-1601PC spectrophotometer. The top-view and cross-section SEM images were obtained from FEI Nova 200 scanning electron microscope. The X-ray diffraction patterns were recorded on a PANalyticalX'Pert Pro Materials Research Diffractometer using Cu Kα radiation. The PL measurement was done by a Hamamatsu Near Infrared Compact Fluorescence Lifetime Spectrometer C12132. The wavelength of the incident light radiation was 532 nm. KPFM scans were obtained with a Bruker Multimode 8, mounting a Pt/Ir coated tip with a nominal spring constant between 1 and 5 nm. Surface potential was detected during an interleave scan at a height of 115 nm over the samples' surface. Photovoltaic characteristics of the devices were measured under a nitrogen atmosphere using a Keithley 2602A Source-Measure Unit and an Abet solar simulator with simulated AM1.5G illumination. The light irradiance was calibrated by an KG5 band pass equipped with ISE Fraunhofer certified Si photodiode. The devices were measured from forward to reverse bias, or from reverse bias to forward bias, with a scan speed of 1 V/s. The EQE was measured with a photospectrometer setup (Bentham PVE300) by illuminating the solar cell with a modulated monochromatic light (Xe and quartz halogen lamps). It is carried out with a chop frequency of 377 Hz but without light bias. The spectral resolution is 5 nm. The steady-state PCEs over illumination time was recorded by loading the devices at the maximum power point identified from the reverse *J-V* scan.

Acknowledgements

W. Qiu would like to acknowledge Ziyang Liu for taking the SEM images. This research has received (partial) funding from the Flemish Government – Department of Economics, Science and Innovation.

References

1 A. Polman, M. Knight, E. C. Garnett, B. Ehrler, W. C. Sinke, *Science*, 2016, **352**, 6283.

2 National Renewable Energy Laboratory (NREL), "Best Research-Cell Efficiencies," can be found under http://www.nrel.gov/ncpv/, 2016.

3 C. Chueh, C. Li, A. K. Jen, *Energy Environ. Sci.* 2015, **8**, 1160.

4 W. Qiu, M. Buffière, G. Brammertz, U. W. Paetzold, L. Froyen, P. Heremans, D. Cheyns, *Org. Electron.* 2015, **26**, 30.

5 M. Saliba, T. Matsui, J.-Y. Seo, K. Domanski, J.-P. Correa-Baena, N. Mohammad K., S. M. Zakeeruddin, W. Tress, A. Abate, A. Hagfeldt, M. Gratzel, *Energy Environ. Sci.* 2016, **9**, 1989.

6 D. Bi, W. Tress, M. I. Dar, P. Gao, J. Luo, C. Renevier, K. Schenk, A. Abate, F. Giordano, J.-P. Correa Baena, J.-D. Decoppet, S. M. Zakeeruddin, M. K. Nazeeruddin, M. Gra tzel, A. Hagfeldt, *Sci. Adv.* 2016, **2**, e1501170.

7 W. S. Yang, J. H. Noh, N. J. Jeon, Y. C. Kim, S. Ryu, J. Seo, S. Il Seok, *Science.* 2015, DOI: 10.1126/science.aaa9272.

8 W. Qiu, U. W. Paetzold, R. Gehlhaar, V. Smirnov, H.-G. Boyen, J. G. Tait, B. Conings, W. Zhang, C. B. Nielsen, I. McCulloch, L. Froyen, P. Heremans, D. Cheyns, *J. Mater. Chem. A* 2015, **3**, 22824.

9 D. Liu, T. L. Kelly, *Nat. Photonics* 2013, **8**, 133.

10 D. P. McMeekin, G. Sadoughi, W. Rehman, G. E. Eperon, M. Saliba, M. T. Hörantner, A. Haghighirad, N. Sakai, L. Korte, B. Rech, M. B. Johnston, L. M. Herz, H. J. Snaith, *Science*, 2016, **351** , 151.

11 S. S. Shin, W. S. Yang, J. H. Noh, J. H. Suk, N. J. Jeon, J. H. Park, J. S. Kim, W. M. Seong, S. Il Seok, *Nat. Commun.* 2015, **6**, 7410.

12 H. Yoon, S. M. Kang, J. K. Lee, M. Choi, *Energy Environ. Sci.*, 2016,**9**, 2262

13 S. Ryu, J. Seo, S. S. Shin, Y. C. Kim, N. J. Jeon, J. H. Noh, S. Il Seok, *J. Mater. Chem. A Mater. energy Sustain.* 2015, **3**, 3271.

14 Y. Shao, Z. Xiao, C. Bi, Y. Yuan, J. Huang, *Nat. Commun.* 2014, **5**, 5784.

15 K. Wojciechowski, T. Leijtens, S. Siprova, C. Schlueter, T. Horantner, J. T. W. Wang, C. Z. Li, A. K. Y. Jen, T. L. Lee, H. J. Snaith, *J. Phys. Chem. Lett.* 2015, **6**, 2399.

16 K. Wojciechowski, S. D. Stranks, A. Abate, G. Sadoughi, H. J. N. Sadhanala, G. Rumbles, C.-Z. Li, R. H. Friend, A. K. Y. Jen, H. J. Snaith, *ACS Nano,* 2014, **8**, 12701.

17 T. Cao, Z. Wang, Y. Xia, B. Song, Y. Zhou, N. Chen, and Y. Li, *ACS Appl. Mater. Interfaces*, 2016, **8**, 18284.

18 Y. Li, Y. Zhao, Q. Chen, Y. Liu, Z. Hong, Z. Liu, Y. Hsieh, L. Meng, Y. Li, Y. Yang, *J. Am. Chem. Soc.*, 2015, **137,** 15540.

19 J. W. Rumer, R. S. Ashraf, N. D. Eisenmenger, Z. Huang, I. Meager, C. B. Nielsen, B. C. Schroeder, M. L. Chabinyc, I. Mcculloch, *Adv. Energy Mater.*, 2015, **5**, 1401426 .

20 M. Saliba, W. Zhang, M. De Bastiani, A. Petrozza, *Mater. Horizons* 2015, **2**, 315.

21 P. Docampo, J. M. Ball, M. Darwich, G. E. Eperon, H. J. Snaith, *Nat. Commun.* 2013, **4**, 2761.

22 J. H. Kim, C.-C. Chueh, S. T. Williams, A. K.-Y. Jen, *Nanoscale* 2015, **7**, 17343.

23 J. H. Heo, H. J. Han, D. Kim, T. K. Ahn, S. H. Im, *Energy Environ. Sci.* 2015, **8**, 1602.

24 G. Xing, N. Mathews, S. Sun, S. S. Lim, Y. M. Lam, M. Grätzel, S. Mhaisalkar, T. C. Sum, *Science*, 2013, **342**, 344.
25 Z. Zhu, Y. Bai, X. Liu, C.-C. Chueh, S. Yang, A. K.-Y. Jen, *Adv. Mater.* 2016, DOI 10.1002/adma.201600619.
26 Z. He, C. Zhong, S. Su, M. Xu, H. Wu, Y. Cao, *Nat Phot.* 2012, **6**, 591.
27 J. T. Jacobsson, J. P. Correa Baena, M. Pazoki, M. Saliba, K. Schenk, M. Grätzel, A. Hagfeldt, *Energy Environ. Sci.* 2016, **41**, 1.
28 N. J. Jeon, J. H. Noh, W. S. Yang, Y. C. Kim, S. Ryu, J. Seo, S. Il Seok, *Nature*, 2015, **517**, 476.
29 W. Qiu, T. Merckx, M. Jaysankar, C. Masse de la Huerta, L. Rakocevic, W. Zhang, U. W. Paetzold, R. Gehlhaar, L. Froyen, J. Poortmans, D. Cheyns, H. J. Snaith, P. Heremans, Energy Environ. Sci. 2016, **9**, 484.

TOC:

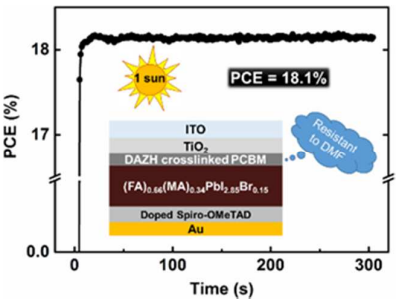

PCBM crosslinked by 1,6-diazidohexane (DAZH) was introduced to solve the solvent incompatibility of depositing solution processed perovskite layer onto it.

Supporting Information

Highly Efficient Perovskite Solar Cells with Crosslinked PCBM Interlayers

W. Qiu, [a, b, †] *J. P. Bastos,* [a, c] *S. Dasgupta,* [a] *T. Merckx,* [a] *I. Cardinaletti,* [d] *M. V. C. Jenart,* [e] *C. B. Nielsen,* [e, f] *R. Gehlhaar,* [a] *J. Poortmans,* [a, c] *P. Heremans,* [a, c, †] *I. McCulloch,* [g] *and D. Cheyns* [a]

[a] *IMEC, Kapeldreef 75, Heverlee, B-3001, Belgium*

[b] *MTM, KU Leuven, Heverlee, Belgium*

[c] *ESAT, KU Leuven, Heverlee, Belgium*

[d] *Hasselt University, IMO-IMOMEC, Diepenbeek, 3590, Belgium*

[e] *Department of Chemistry and Centre for Plastic Electronics, Imperial College London, SW7 2AZ, UK*

[f] *Materials Research Institute and School of Biological and Chemical Sciences, Queen Mary University of London, Mile End Road, London E1 4NS, UK*

[g] *Physical Sciences and Engineering Division, King Abdullah University of Science and Technology (KAUST), Thuwal 23955-6900 , Saudi Arabia*

[†] *Corresponding author: Weiming.Qiu@imec.be; Paul.Heremans@imec.be*

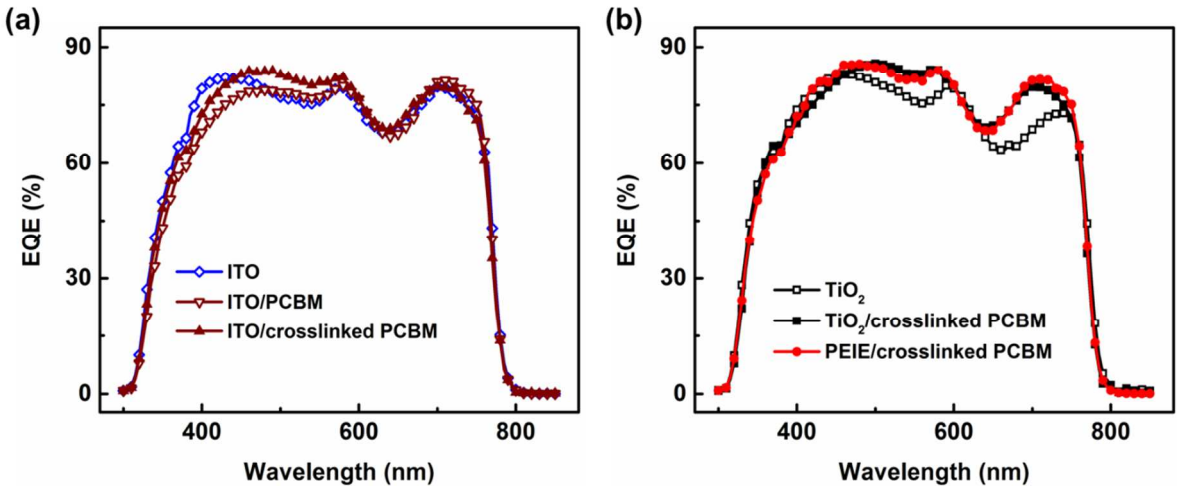

Fig. S1 (a) the EQE curves of of the PSCs without ETL, with pristine PCBM and with crosslinked PCBM as ETL; (b) The EQE curves of PSCs with TiO_2, TiO_2/crosslinked PCBM, PEIE, PEIE/crosslinked PCBM as ETL.

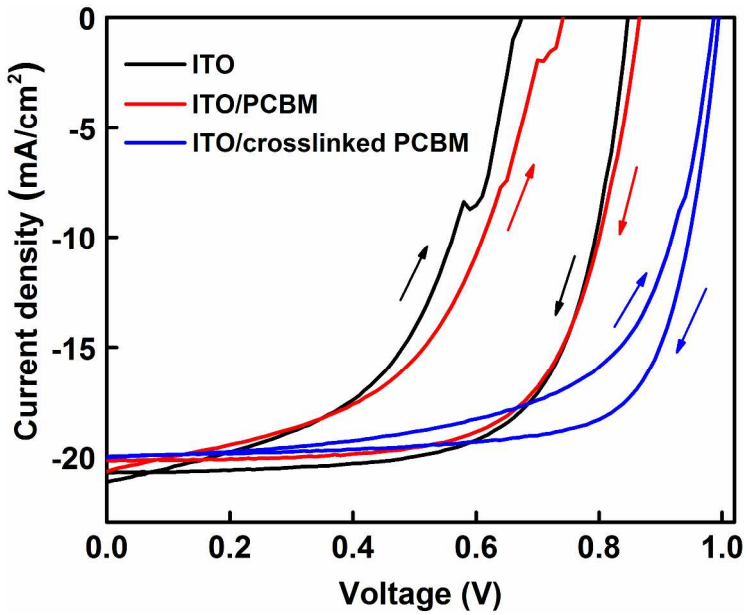

Fig. S2 The *J-V* curves from both reverse and forward sweep of perovskite solar cells with different ETLs.

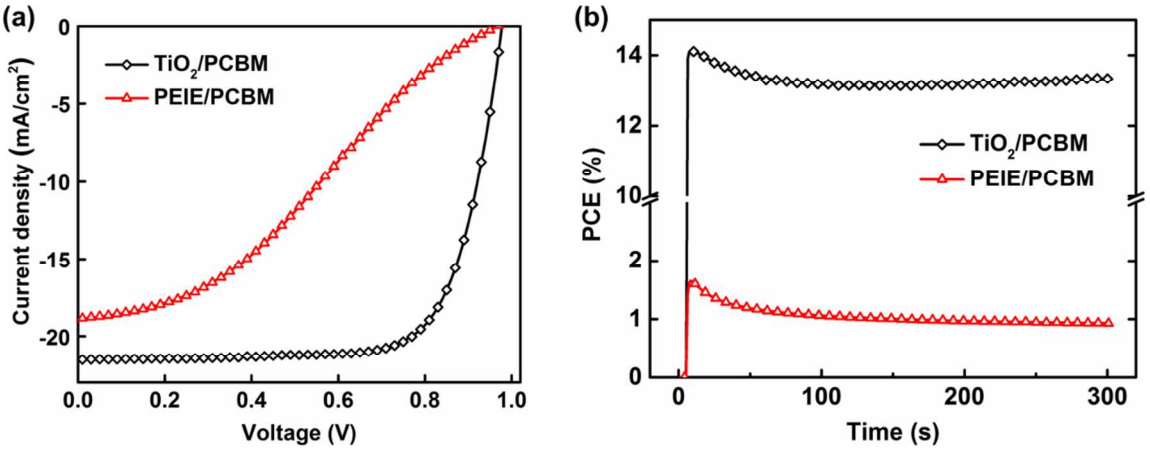

Fig. S3 (a) The *J-V* curves and (b) the steady-state PCEs of PSCs with TiO_2/PCBM and PEIE/PCBM as the ETL, respectively

Table S1. The detailed photovoltaic parameters of the perovskite solar cells using TiO_2/PCBM and PEIE/PCBM as the ETL, respectively, with the data extracted from Fig. S3.

ETLs	J_{sc} (mA/cm^2)	V_{oc} (V)	FF (%)	PCE_{jv} (%)	PCE_{bias} (%)	Irradiance (mW/cm^2)
TiO_2/PCBM	21.5	0.98	73.2	15.4	13.3	100
PEIE/PCBM	18.9	0.97	33.0	6.0	0.9	100

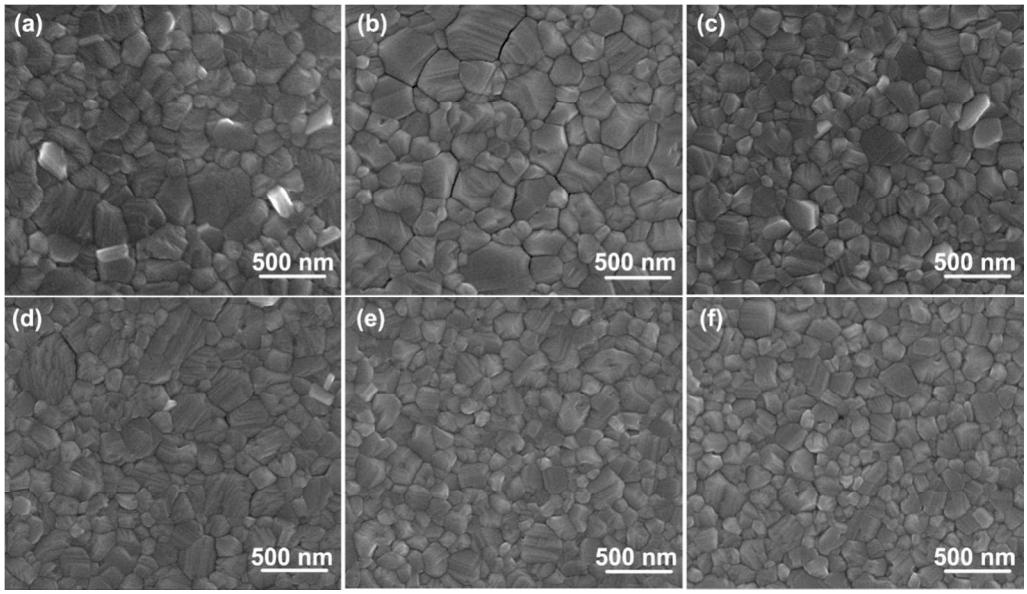

Fig. S4 Top-view SEM images of $CH_3NH_3PbI_3$ films deposited on (a) ITO, (b) TiO_2, (c) PEIE, (d) crosslinked PCBM, (e) TiO_2/crosslinked PCBM, (f) PEIE/crosslinked PCBM.

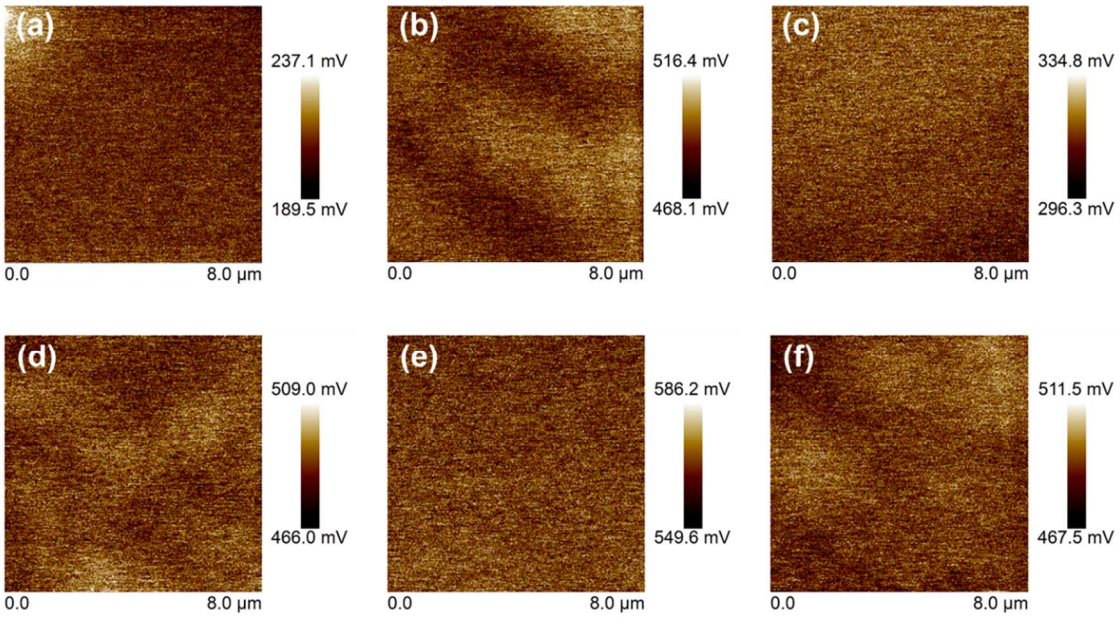

Fig. S5 Difference between the tip work function and that of different ETLs on ITO substrates: (a) ITO; (b) Crosslinked PCBM; (c) TiO_2; (d) TiO_2/crosslinked PCBM; (e) PEIE; (f) PEIE/crosslinked PCBM. The work function of the different tips used was not perfectly matching, therefore whenever the tip needed to be changed, we would re-acquire the potential for the last measured layer, as to be able to fix the offsets to the same scale. This explains eventual incongruences between the data in **Fig. 3d** and that in the scan images.

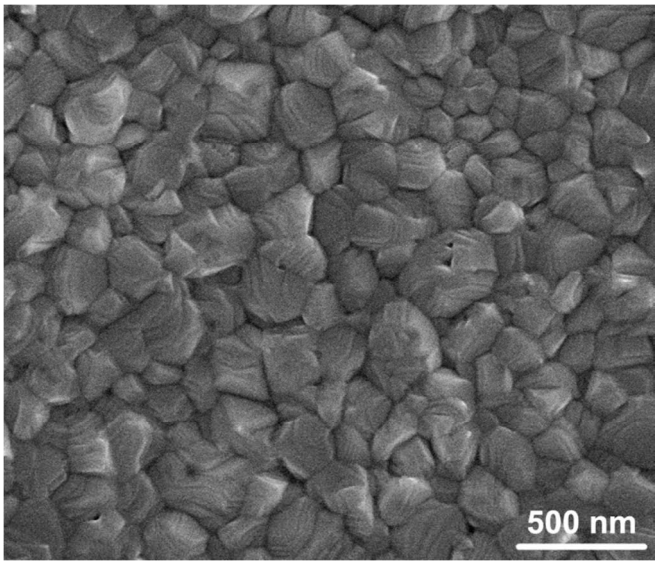

Fig. S6 Top-view SEM images of the $(HC(NH_2)_2)_{0.66}(CH_3NH_3)_{0.34}PbI_{2.85}Br_{0.15}$ film deposited on TiO_2/crosslinked PCBM ETL.

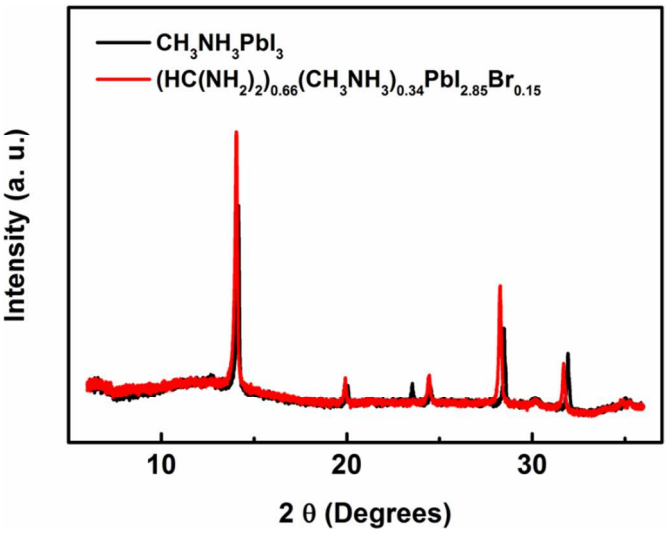

Fig. S7 XRD patterns of the $CH_3NH_3PbI_3$ and $(HC(NH_2)_2)_{0.66}(CH_3NH_3)_{0.34}PbI_{2.85}Br_{0.15}$ films deposited on TiO_2/crosslinked PCBM ETL

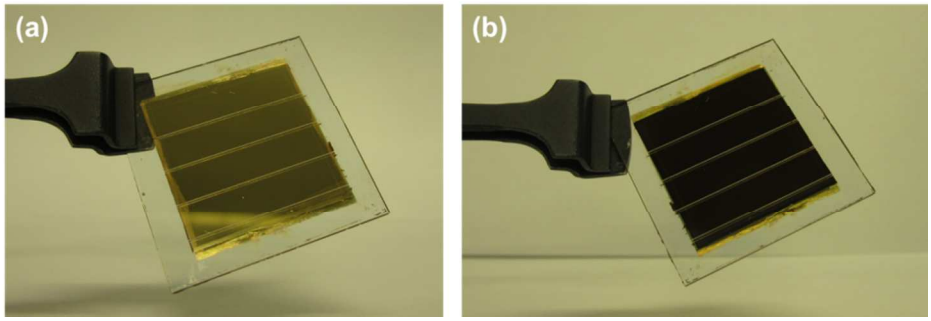

Fig. S8 Digital images of our perovskite module taken from (a) the metal electrode side and (b) the ITO side. It has a total aperture area of 4 cm^2, with 4 sub-cells.

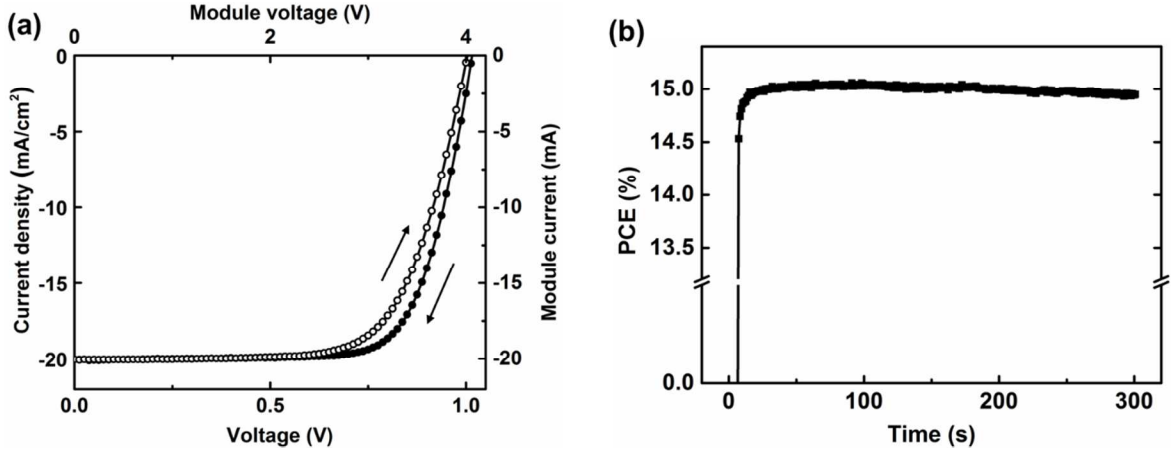

Fig. S9 (a) the J-V curves and (b) the steady-state PCE of the perovskite solar module.